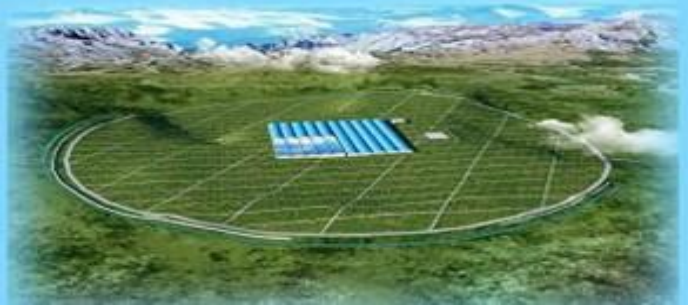

Large High Altitude Air Shower Observatory

耀变体关联辐射及其高能辐射区位置

戴本忠
云南大学

Outline

- Blazars
- Multiband observations
- Location of high energy emission
- Summary and outlook

耀变体及其基本性质

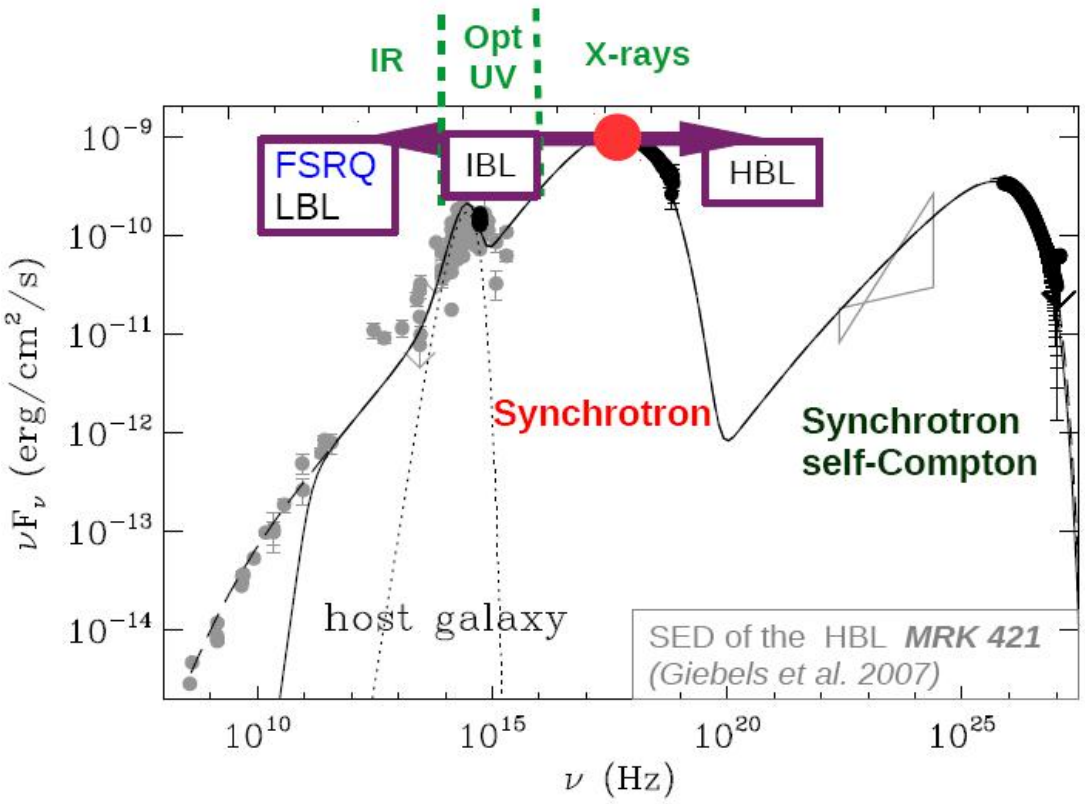

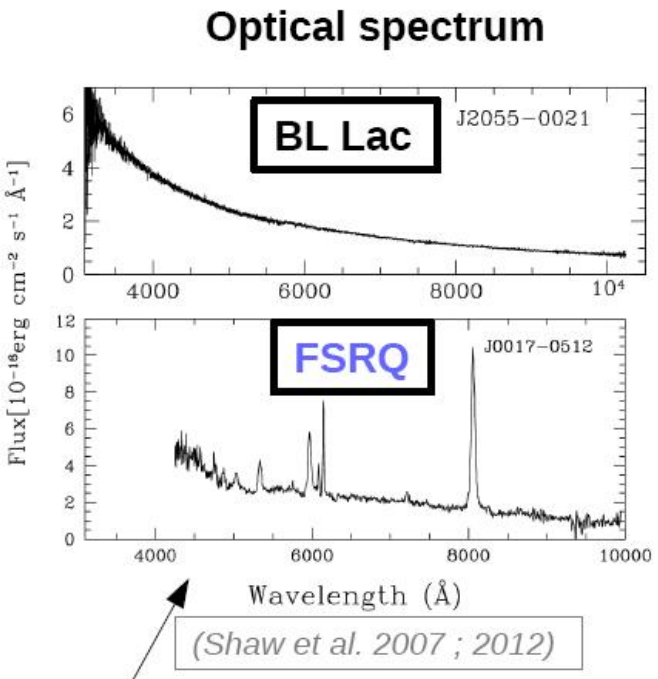

Strong BLR and accretion disk

Blazars:耀变体所具有的剧烈光变及喷流指向等性质，使其成为通过多波段能谱及光变特征研究活动星系核喷流中潜在的物理机制最重要的对象。

Petropoulou MNRAS **452, 1303–1315 (2015)**

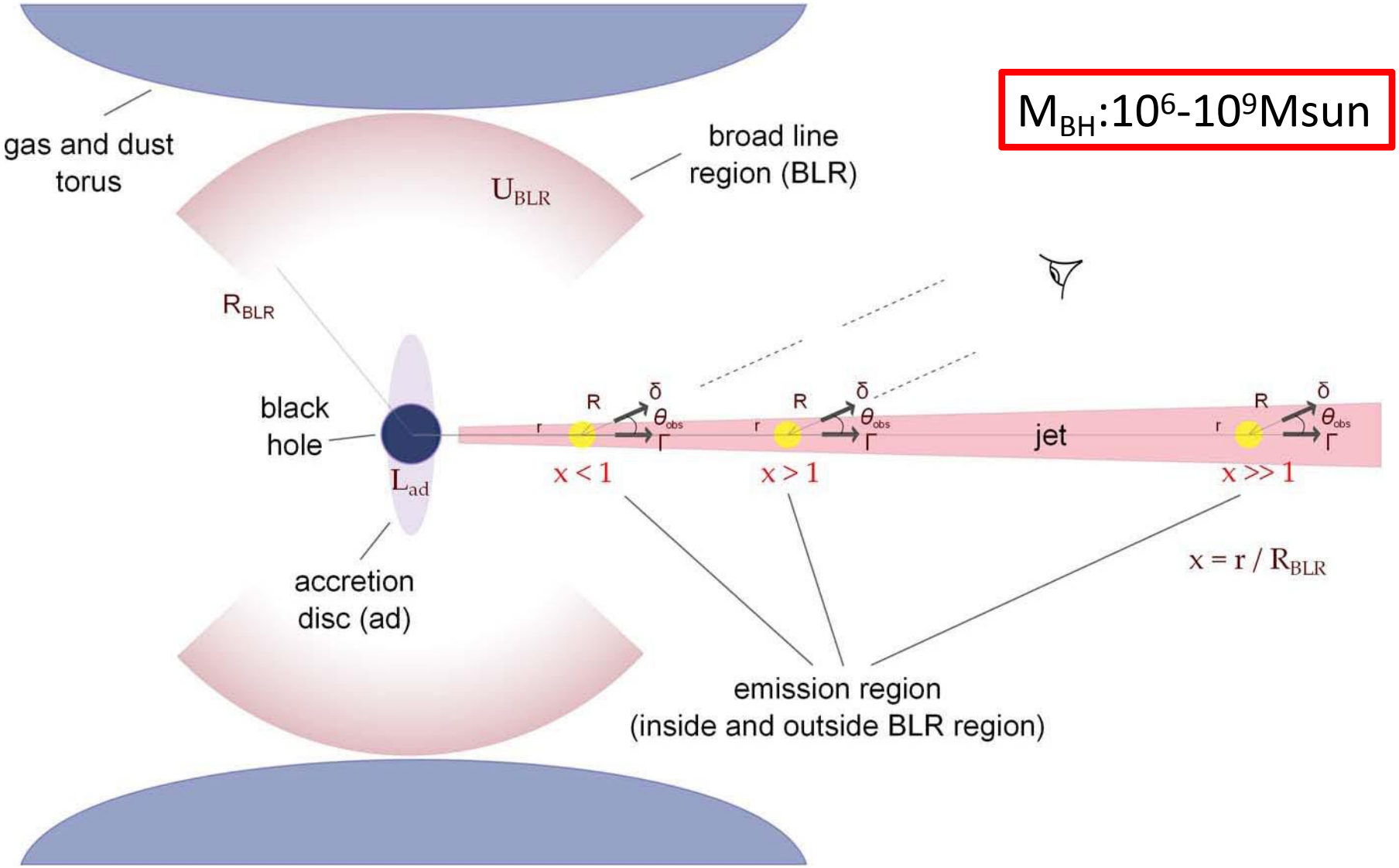

M_{BH}:10^6-10^9Msun

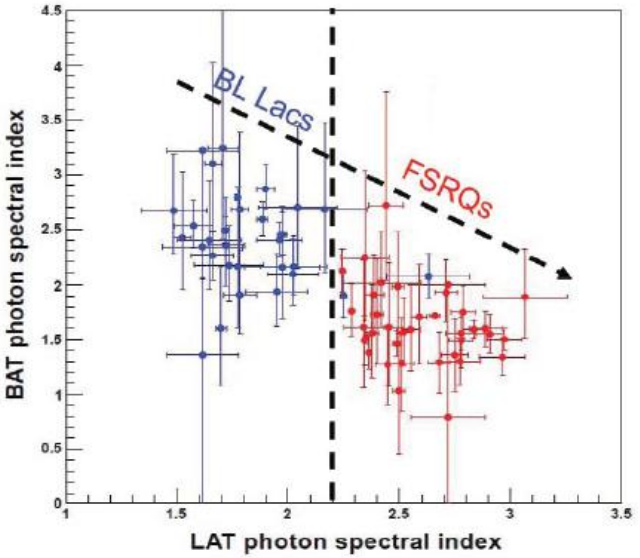

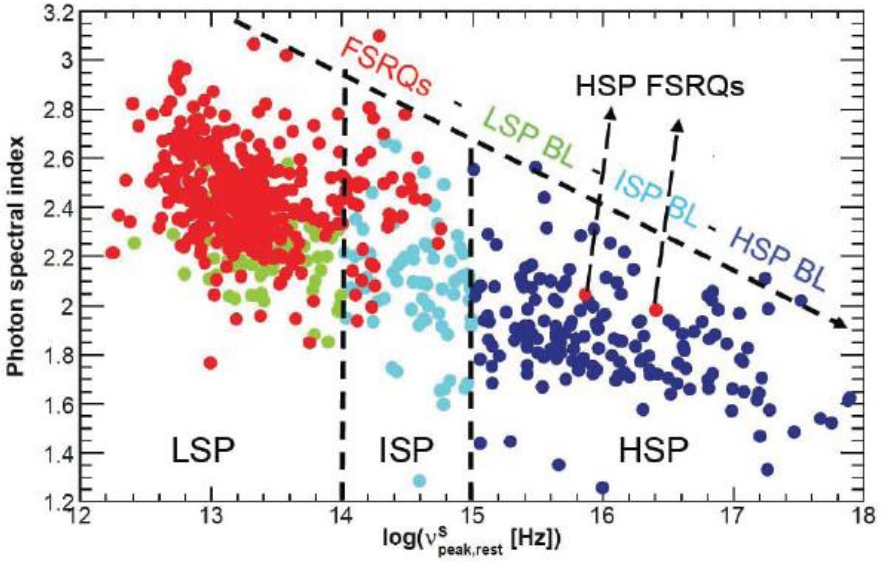

- RBLs & XBLs
- LBLs， IBLs & HBLs （同步辐射峰频）
- LSP， ISP & HSP
- lLSP (low-synchrotron-peaked blazar, $< 10^{14}$ Hz)
- ISP (intermediate-synchrotron-peaked blazar, 10^{14} Hz - 10^{15} Hz)
- HSP (high-synchrotron-peaked blazar , $> 10^{15}$ Hz)

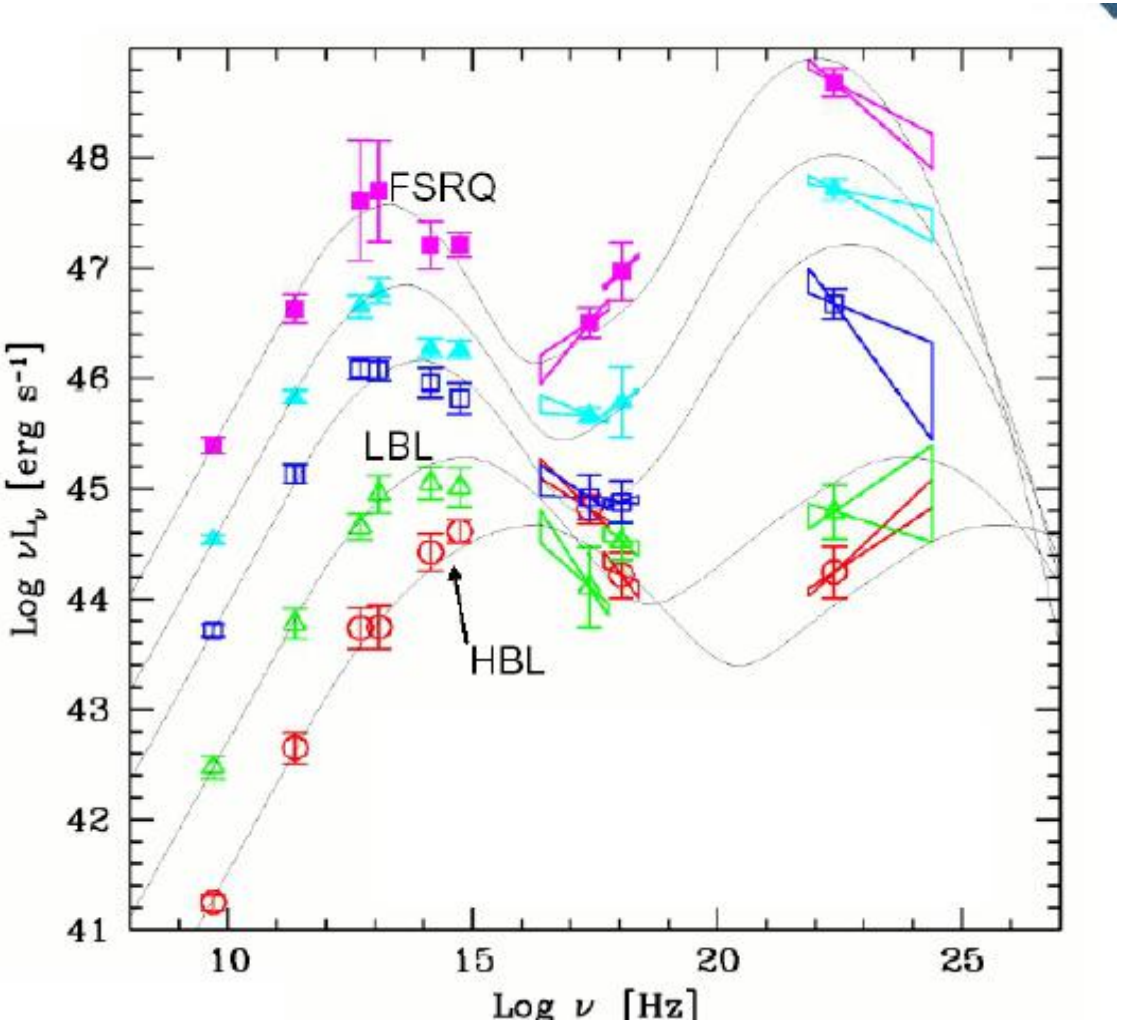

耀变体SED

Fossati et al., 1998;

Donato et al., 2001

- 根据射电流量大小，将Blazar划分为5部分，每一部分的平均能谱分布均具有双峰结构，并且具有随光度增加其峰值频率向低能移动的趋势。

Multiband observations

- More than 100 years in optical band
- Radio, from 2.3GHz to mm/submm (SMA)
- X-ray, keV to few hundred keV, ASCA, RXTE, Swift, Chandra, NuStar
- GeV, EGRET to Fermi
- TeV, HESS, VERITAS, MAGIC, ARGO-YBJ and LHAASO

- 获得从射电到TeV甚高能全波段能谱

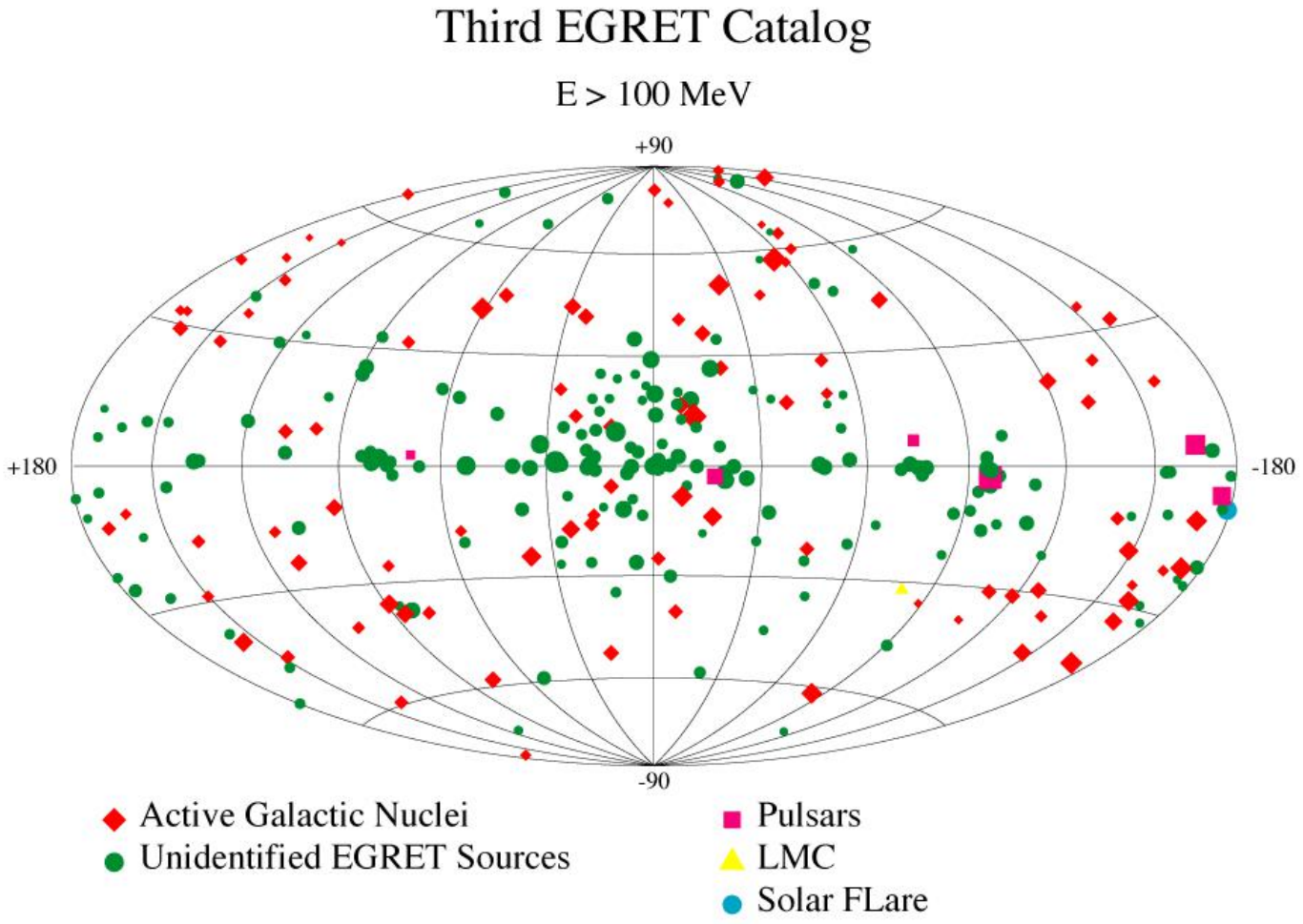

3. EGRET Catalog: (3EG)
Hartman et al, 1999
ApJS, 123, 79

271 Sources
80-90 AGN
67 Blazars
6-8 PSR
~170 Unid..

1. COMPTEL Catalog:
Schönfelder et al., 2000
A&AS, 143, 145

32 constant Sources.
39 transient
11 AGN
3 PSR
4 EGRET Unid.

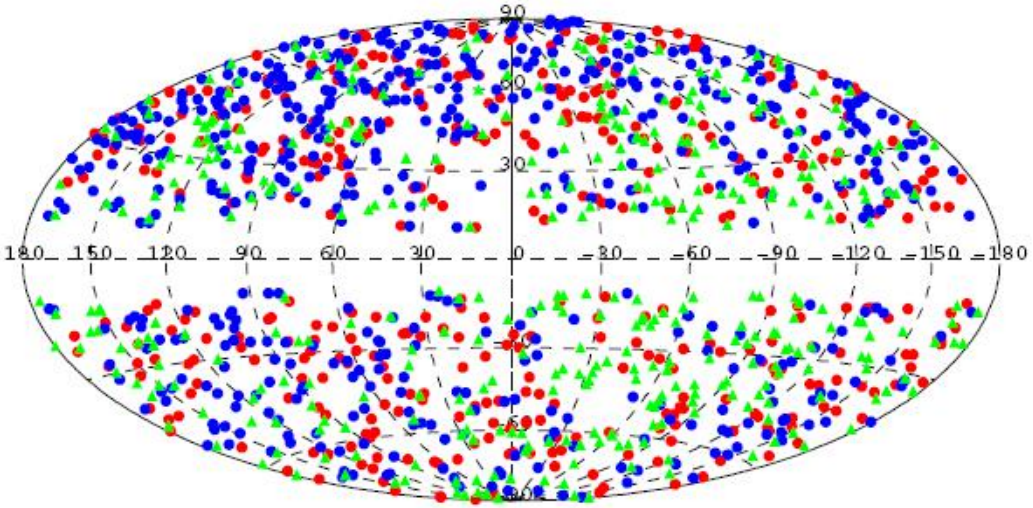

The Third Catalog of Active Galactic Nuclei Detected by the Fermi Large Area Telescope， Ackermann, et al, 2015, ApJ, 810,14

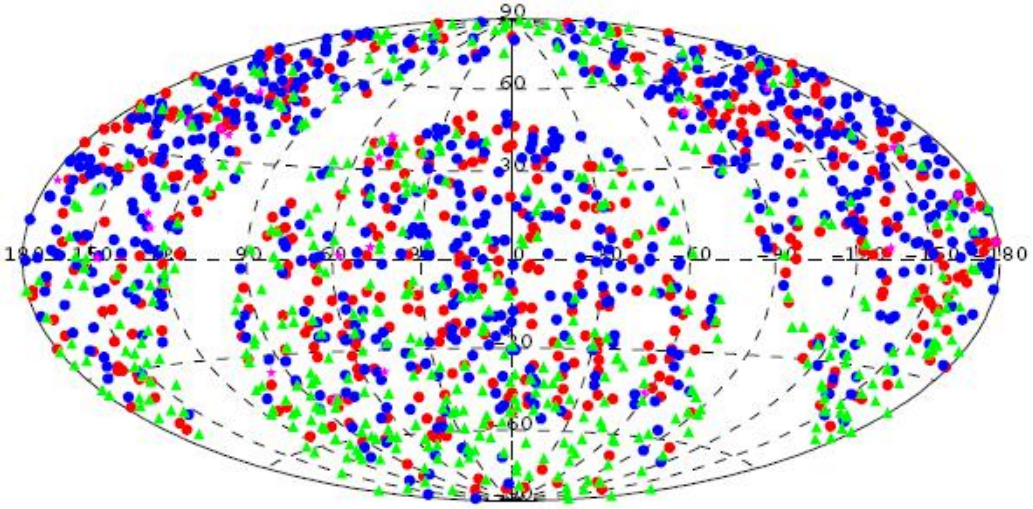

Fig. 5.— Locations of the sources in the Clean Sample in Galactic (top) and celestial (bottom) coordinates. Red: FSRQs, blue: BL Lacs, magenta: radio galaxies, green: AGNs of unknown type.

- 1591 blazars, 467 FSRQs,
- 632 BL Lacs
- BCU 460

AGN type	Entire 3LAC	3LAC Clean Sample[a]	Low-latitude sample
All	**1591**	**1444**	**182**
FSRQ	**467**	**414**	**24**
...LSP	412	366	24
...ISP	47	42	0
...HSP	3	2	0
...no SED classification	5	4	0
BL Lac	**632**	**604**	**30**
...LSP	162	150	8
...ISP	178	173	6
...HSP	272	265	12
...no SED classification	20	16	4
Blazar of Unknown type	**460**	**402**	**125**
...BCU I	57	49	11
...LSP BCU I	26	24	8
...ISP BCU I	11	9	1
...HSP BCU I	13	13	2
...BCU I w/o SED classification	7	3	0
...BCU II	346	308	85
...LSP BCU II	156	129	39
...ISP BCU II	78	70	13
...HSP BCU II	107	105	31
...BCU II w/o SED classification	5	4	2
...BCU III	57	45	29
...LSP BCU III	16	11	9
...ISP BCU III	0	0	0
...HSP BCU III	0	0	0
...BCU III w/o SED classification	41	34	20
Non-blazar AGN	**32**	**24**	**3**
...CSS	2	1	0
...NLSy1	5	5	0
...RG	14	13	2
...SSRQ	5	3	0
...Other AGN	6	2	1

Hard Fermi-LAT Sources (2FHL)

Ackermann, 2015, arXiv:1508.04449

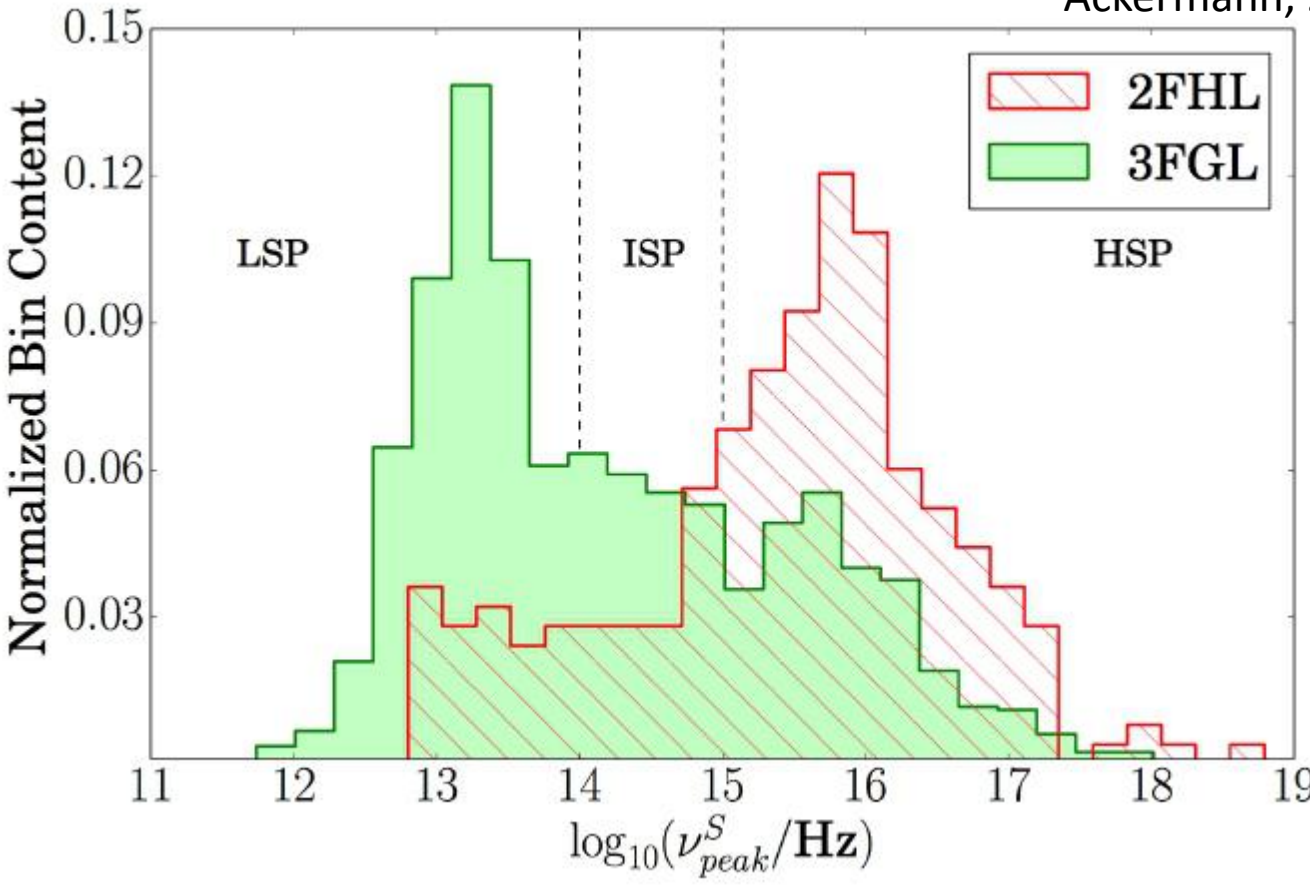

opens a new window on the high-energy sky

360 sources detected between 50 GeV and 2 TeV, 75% blazars, only 25% detected in TeVCat. Most of them are BL Lacs, only 10 FSRQs.

This catalog of sources provides a bridge between the traditional 0.1–100GeV band of *Fermi –LAT* catalogs and the >100GeV band probed by IACTs and other instruments from the ground. It connects well to the TeV world

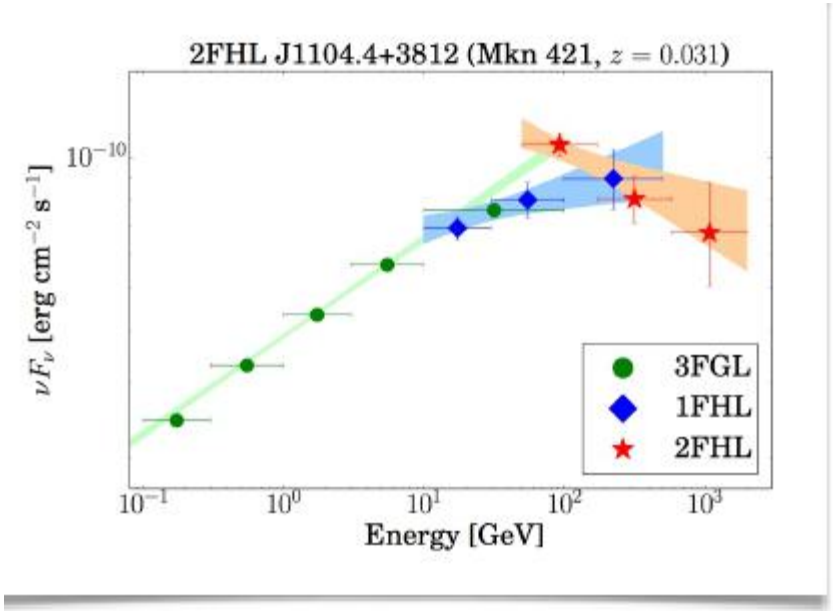

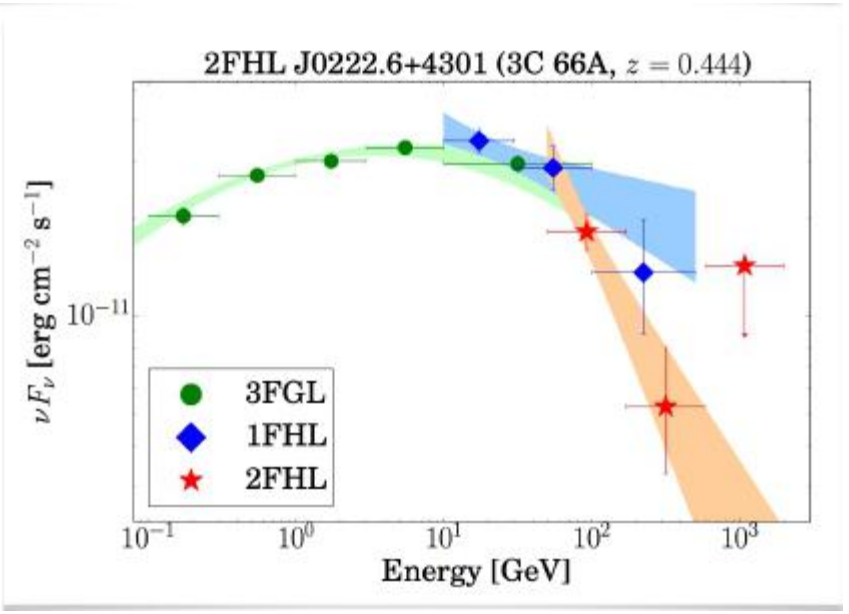

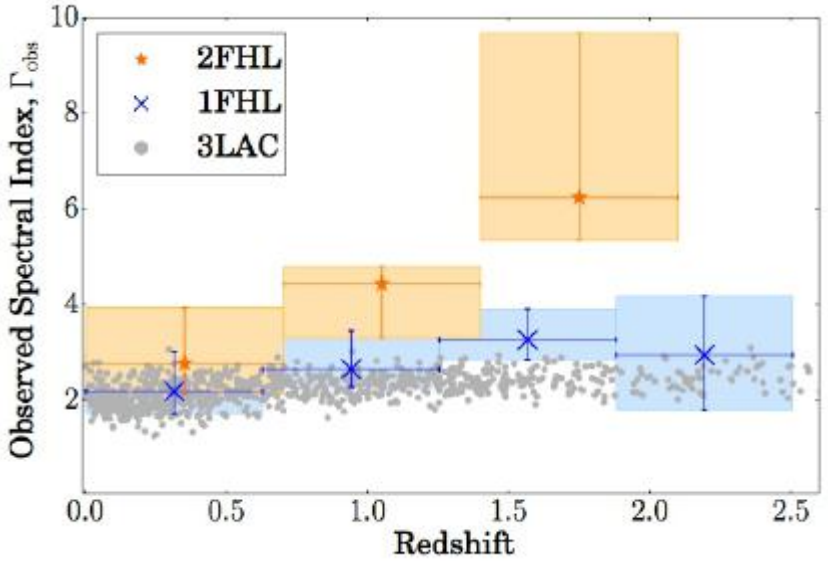

Sources become softer at higher energies

Sources becomes softer at high redshift, most likely due to EBL

66 TeV extragalactic:
FSRQs 5， LBLs 2, IBLs 8,HBLs 46, FRI 4, Blazar 1,

http://tevcat.uchicago.edu

TeV arrays: E>100 GeV

The ARGO-YBJ experiment

An unconventional EAS-array exploiting the full coverage approach at very high altitude to detect small air showers at an energy threshold of a few hundreds of GeV.

Longitude 90° 31' 50" East
Latitude 30° 06' 38" North

90 Km North from Lhasa (Tibet)

4300 m above the sea level
~ 600 g/cm2

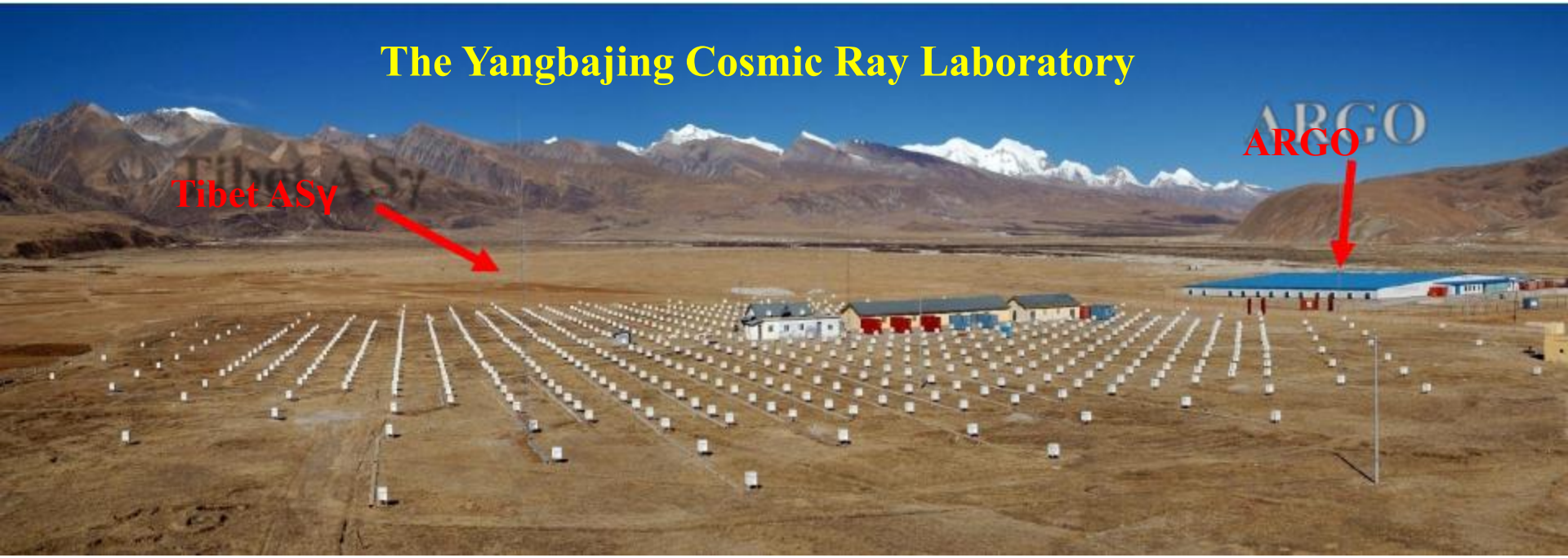

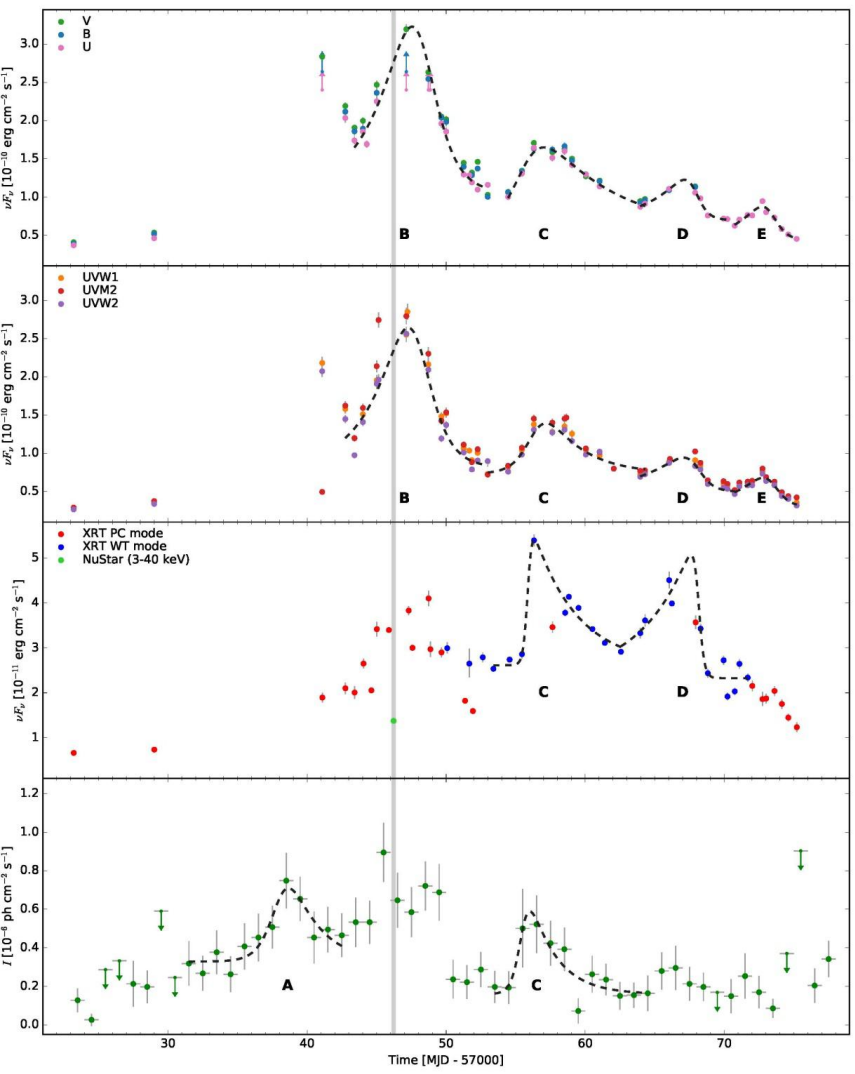

PKS 0716+714

Wierzcholska

arXiv:1605.00630

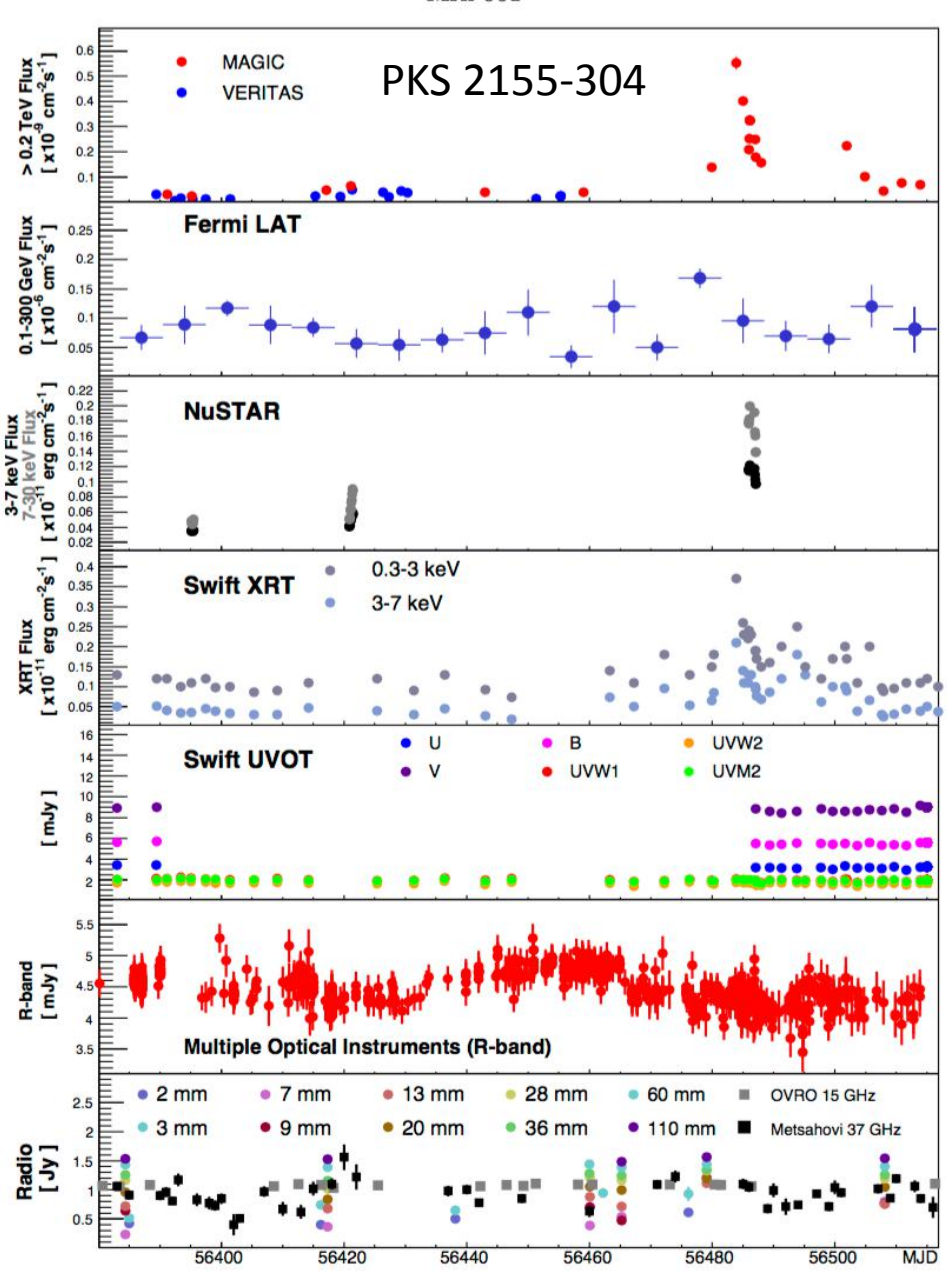

Furniss et al. (2015)

MW campaign on PKS 2155-304

First simultaneous SED including GeV-TeV

Unexpected correlations:

- strong correlation between optical and TeV fluxes
- X-ray flux varies independently of TeV flux
- correlation between X-ray flux and GeV photon index

Challenge simple SSC models

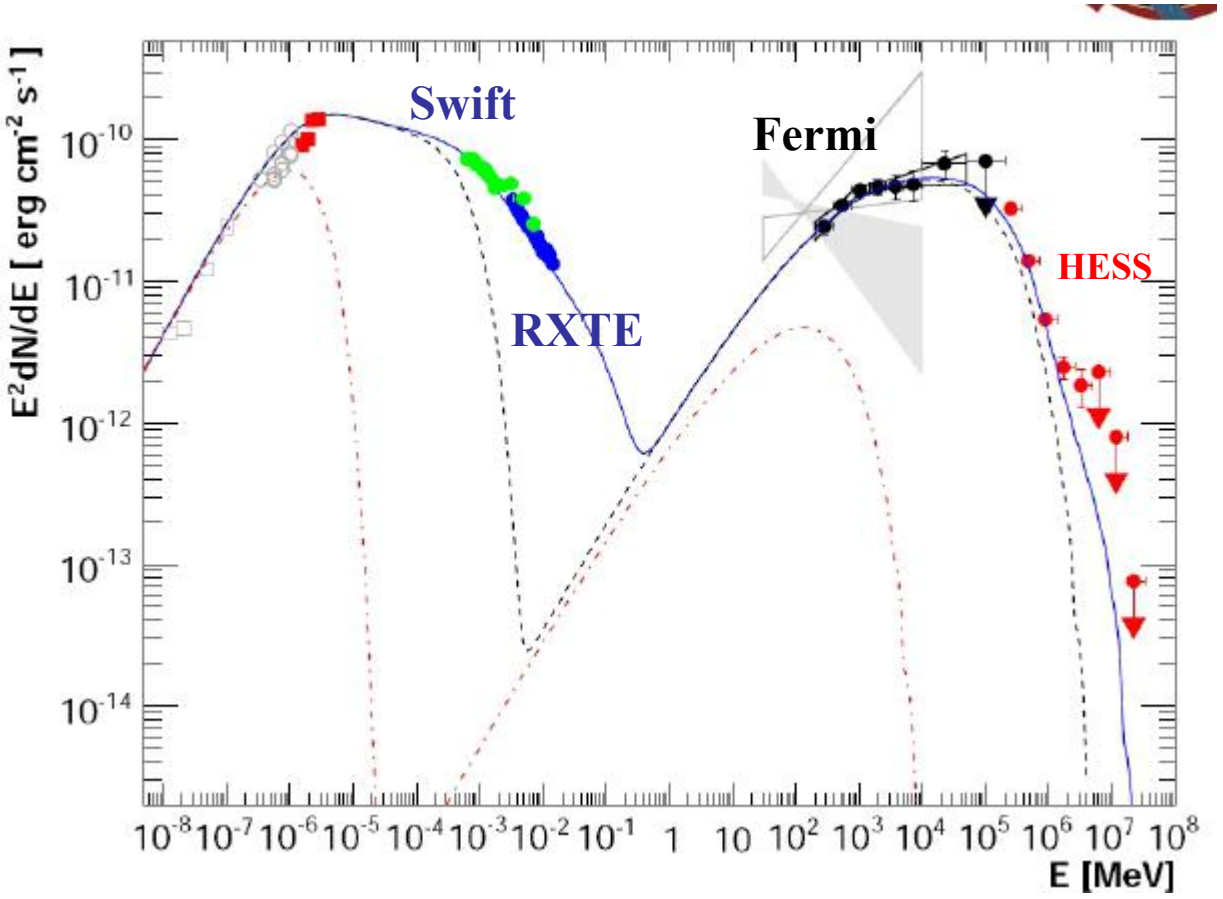

Aharonian, F. et al. 2009, ApJL, 696 L150

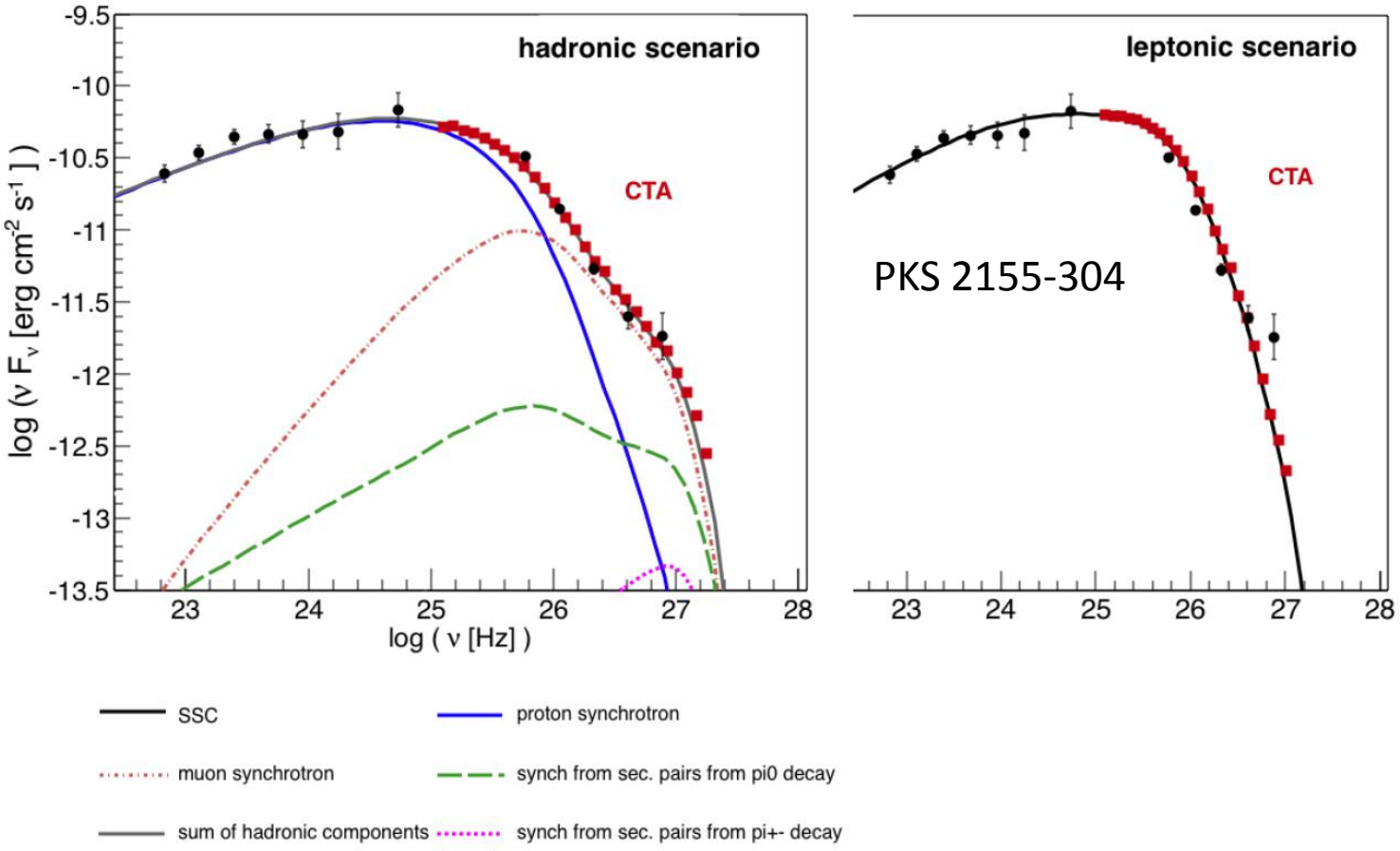
hadronic scenario
leptonic scenario
CTA
CTA
PKS 2155-304
log (ν F_ν [erg cm^-2 s^-1])
log (ν [Hz])
SSC
proton synchrotron
muon synchrotron
synch from sec. pairs from pi0 decay
sum of hadronic components
synch from sec. pairs from pi+- decay

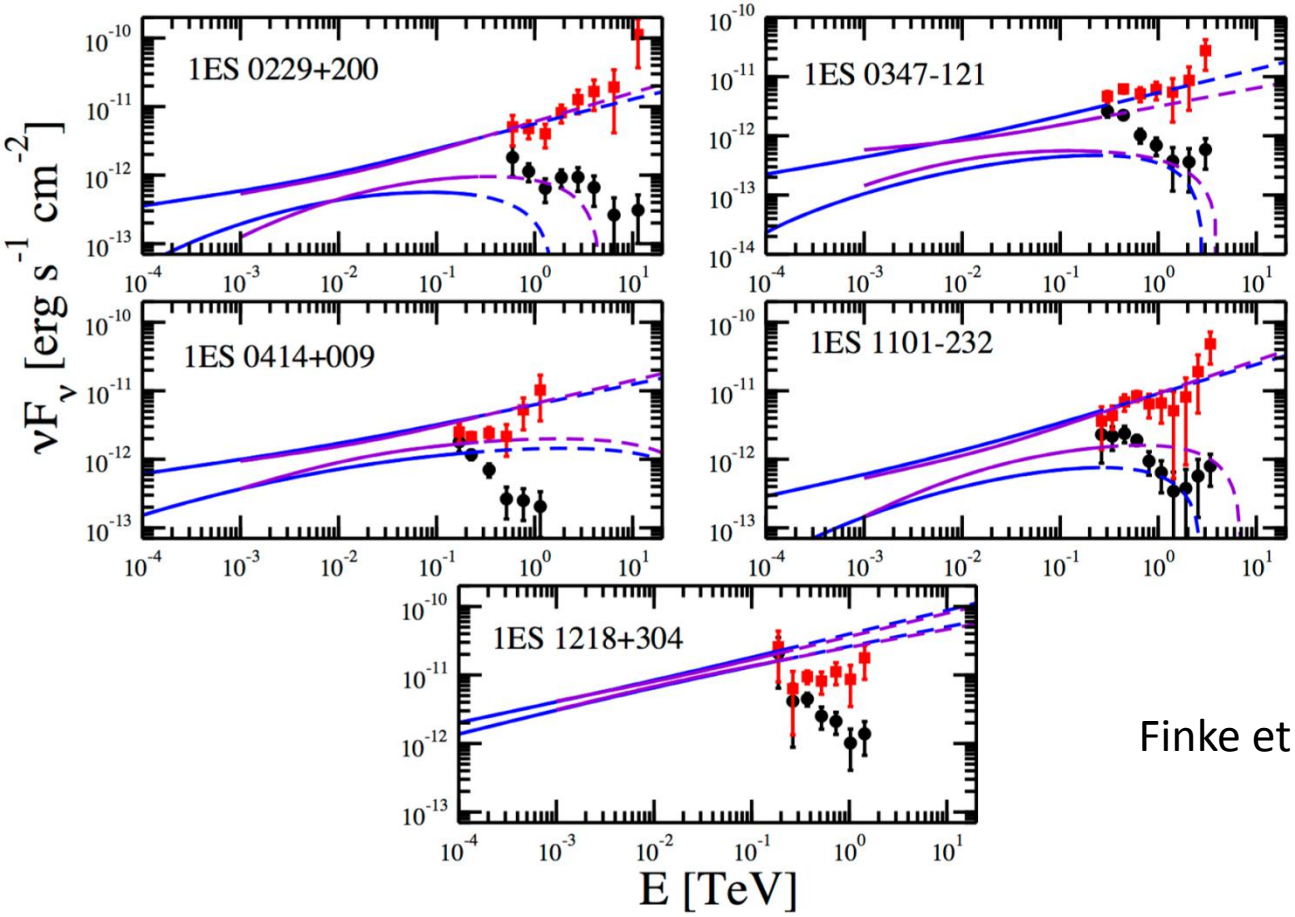

Finke et al., 2015

– The γ-ray spectra for the sources. Blue (violet) curves indicate the LAT spectra at > 0.1 (1.0) GeV, dashed curves indicate the
:tra extrapolated into the VHE region. Circles indicate the observed VHE spectrum from ground-based atmospheric Cherenkov
s, and squares indicate the VHE spectrum deabsorbed with the EBL model of Finke et al. (2010).

Absence of GeV emission from distant blazars: constraints on intergalactic magnetic field

耀变体高能辐射—3C 454.3

3C 454.3，红移 z=0.859，全波段电磁辐射都持续着非常活跃的状态。是第一个发现 GeV 伽玛射线谱存在拐折的伽玛射线源，并存在越亮越硬的趋势。

- 多波段能谱拟合

黑洞质量： $5 \times 10^8 M_\odot$ Bonnoli et al. (2011)

吸积盘光度：$L_{\rm d} \sim 3 \times 10^{46}$ erg s^{-1} (Raiteri et al. 2007)

宽线区光度：$L_{\rm BLR} \sim 3 \times 10^{45}$ erg s^{-1} (Pian et al. 2005, 2006)

model

- 辐射机制：SYN + SSC + EC
  - （1）吸积盘光子
  - （2）宽线区光子

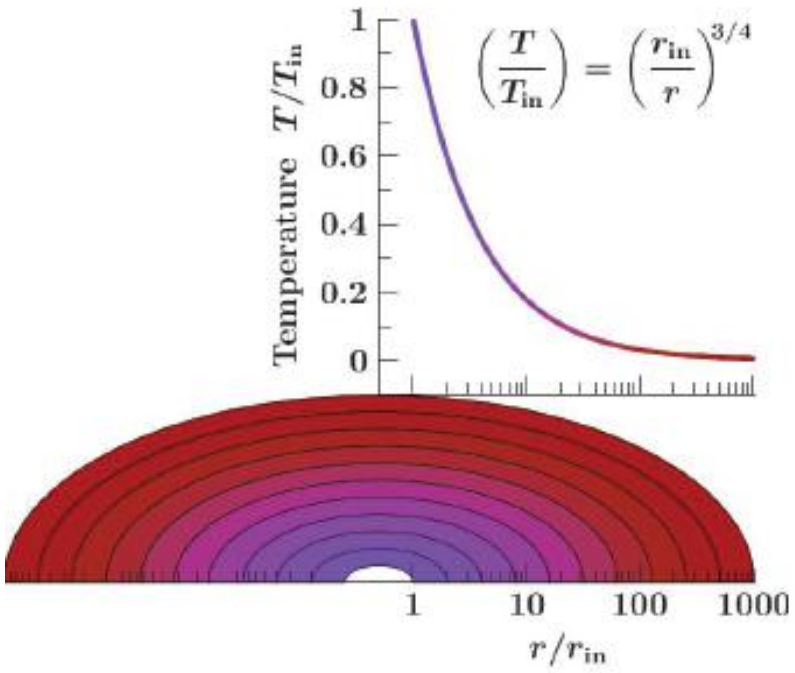

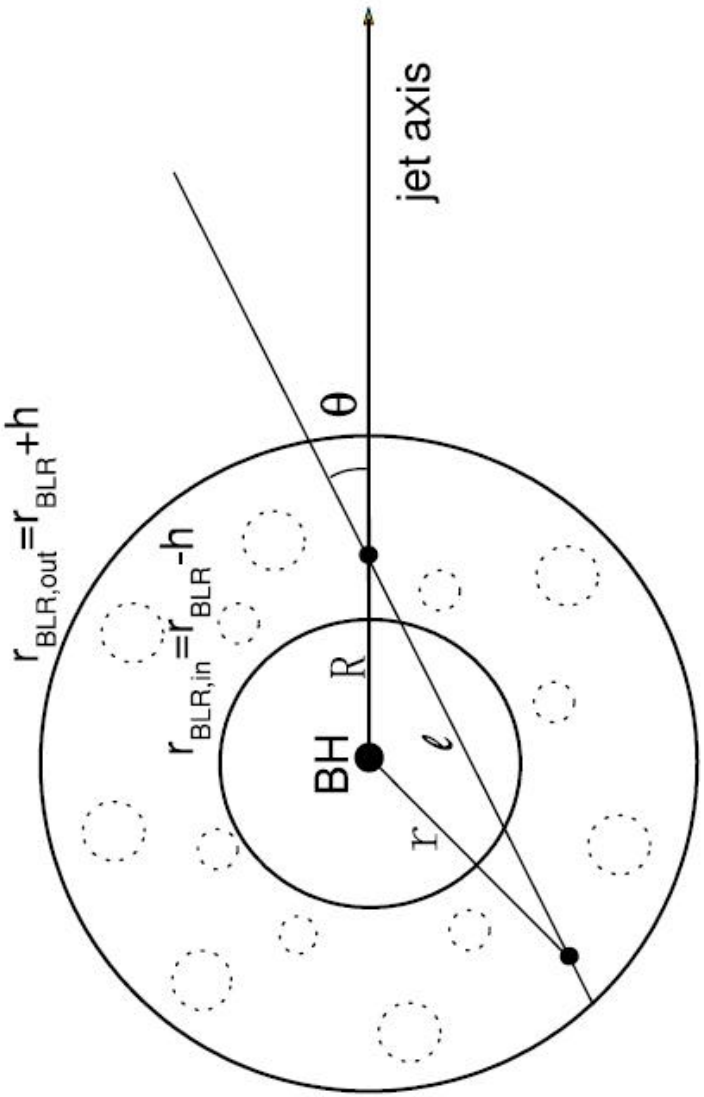

多波段拟合

	Units	06/11	27/11
$\delta_{\rm b}$		13.8	21.3
B'		5.98	2.66
$K'_{\rm e}$			
p_1			
p_2			
$\gamma'_{\rm min}$			
$\gamma'_{\rm b}$			
$t_{\rm var}$			
$z_{\rm b}$			
Cost dc			
lg $R'_{\rm b}$			5.99
$U'_{\rm e}$			26
lg L_B			5.23
lg $L_{\rm e}$			4.83
lg $L_{\rm p}$			5.17
lg L_r			5.48
η			15

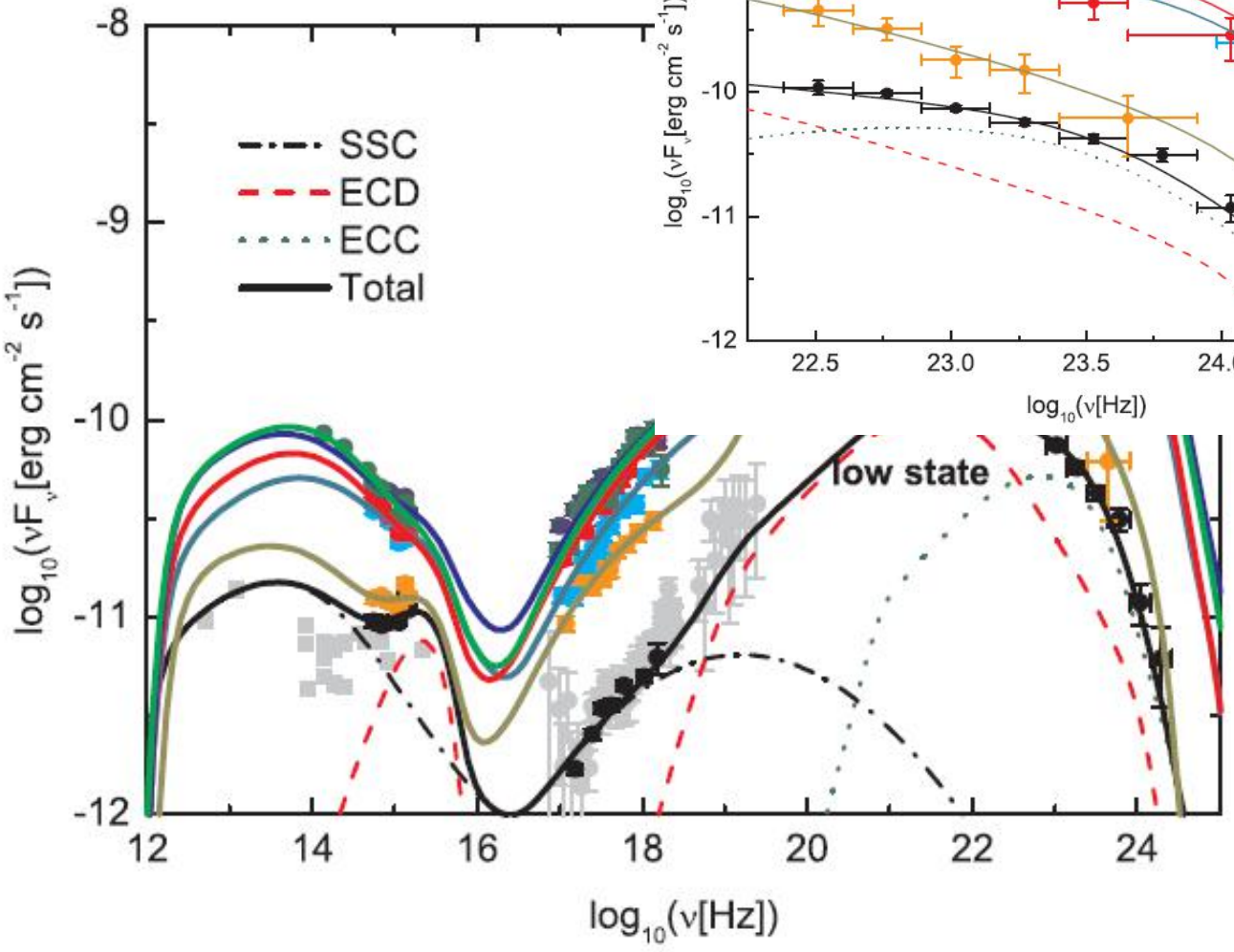

多波段拟合

Hu & Dai 2015

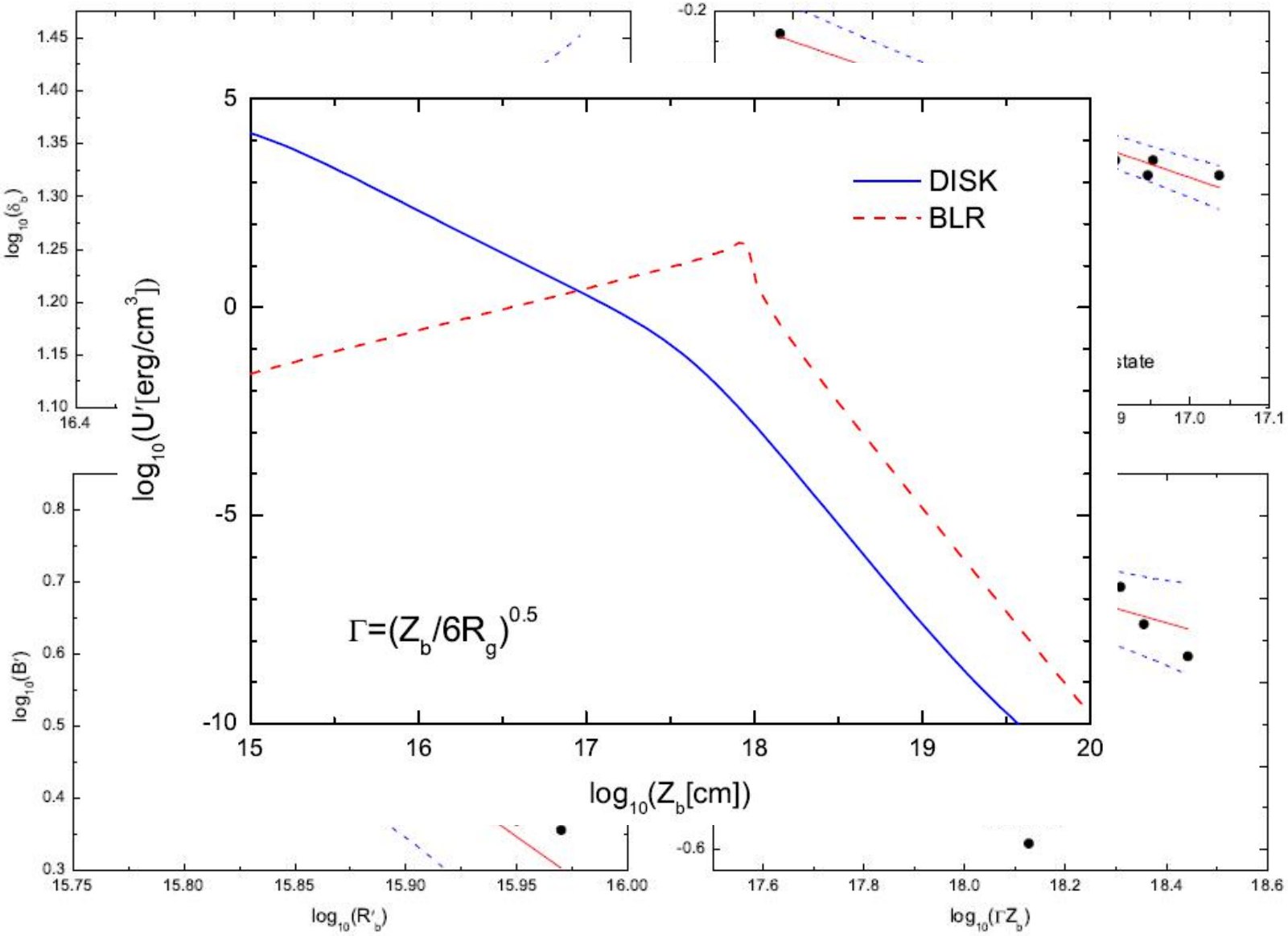

- 耀变体 3C454.3 剧烈的耀发活动可能是由多普勒因子的变化产生的，其多波段非热辐射可能来自于一个新的辐射区的喷射。
- 辐射区，沿着喷流向外运动，辐射效率、相对论性电子和磁场的能量密度不断减小，同时辐射区半径和多普勒因子逐渐增加，逆康普顿散射宽线区光子相对于逆康普顿散射的吸积盘光子对伽玛射线波段的贡献也在增加。
- 自洽的解释观测的伽玛射线谱“越亮越硬”的趋势

耀变体高能辐射—辐射区位置

1）辐射区的位置（sub-pc, supra-pc or >10 pc?），e.g. γ射线吸收，光变特征及相对于光学、射电辐射的延迟.

2）宽线区的物理性质一般通过反响映射技术测量 。但是这种方法要求大量的、高质量的，并且具有明显光变特征的连续辐射及发射线的观测数据。喷流周围物质分布几何结构（尤其是宽线区的几何结构: spherical or flat?）

通过27个耀变体多波段准同时性或同时性能谱得到中心黑洞质量、吸积率、外部辐射场的能量密度及辐射区位置。

❖ 均分的喷流辐射模型

- 电子谱分布：截断幂率谱

$$n'_e(\gamma') = k'_e \begin{cases} (\gamma'/\gamma'_b)^{-p_1} & \text{for } \gamma'_{min} \le \gamma' \le \gamma'_b \\ (\gamma'/\gamma'_b)^{-p_2} & \text{for } \gamma'_b < \gamma' \le \gamma'_{max} \end{cases} .$$

- 能均分关系：

Hu & Dai 2016

$$u'_e = \xi_e U'_B = m_e c^2 \int_{\gamma'_{min}}^{\gamma'_{max}} \gamma' n'_e(\gamma') d\gamma' .$$

- 辐射机制：SYN + SSC + EC

  （a）吸积盘光子 + 宽线区光子 （Model A）

  （b）宽线区光子 + 尘埃光子(Model B)

注意:我们并不考虑外部环境详细的几何结构.

[1]	[2]	[3]	[4]	[5]	[6]	[7]	[8]	[9]	[10]	[11]	[12]	[13]	[14]	[15]
Name	z	M_8	L_d	ν_{sy}^{pk}	ν_{SSC}^{pk}	L_{sy}^{pk}	ξ_s	γ'_{min}	γ'_{max}	p_1	p_2	U_{BLR}	U_{DT}	R_{diss} pc
S4 0133+47														90×10^{-1}/14.50
PKS 0208-51														$.30\times10^{-1}$/7.32
PKS 0227-36														1.1×10^{-1}/4.99
4C 28.07														$.00\times10^{-1}$/6.55
PKS 0347-21														$.7\times10^{-1}$/12.63
PKS 0420-01														3.0×10^{-2}/4.38
PKS 0454-23														3.5×10^{-2}/3.73
PKS 0528+1														$.20\times10^{-1}$/3.43
PKS 0537-44														70×10^{-1}/10.56
PKS 0727-11														$.00\times10^{-2}$/4.03
OJ 287														5.0×10^{-2}/3.94
S4 0917+44														$.65\times10^{-1}$/5.89
4C 01.28														$.00\times10^{-1}$/6.47
4C 29.45														$.50\times10^{-2}$/1.79
3C 273														$.70\times10^{-2}$/1.79
3C 279														$\times10^{-1}$/6.68
1Jy 1308+326														$\times10^{-2}$/4.57
PKS 1454-354														$\times10^{-1}$/8.92
PKS 1502+106														$\times10^{-1}$/7.78
PKS 1510-089														$\times10^{-2}$/0.83
B2 1520+31														$\times10^{-2}$/2.56
OT 081														$\times10^{-2}$/1.22
4C 66.20														$\times10^{-1}$/10.78
S3 2141+17														$\times10^{-2}$/0.30
3C 454.3														$\times10^{-2}$/4.47
PKS 2325+093														$\times10^{-2}$/2.04
PMN 2345-155														$\times10^{-2}$/1.41

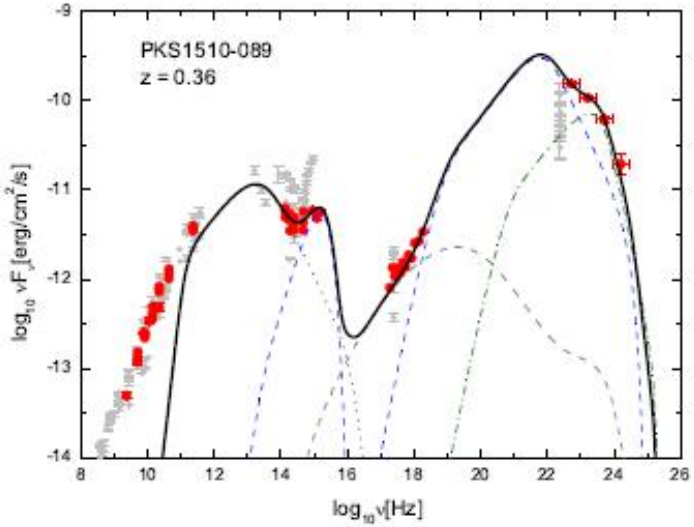

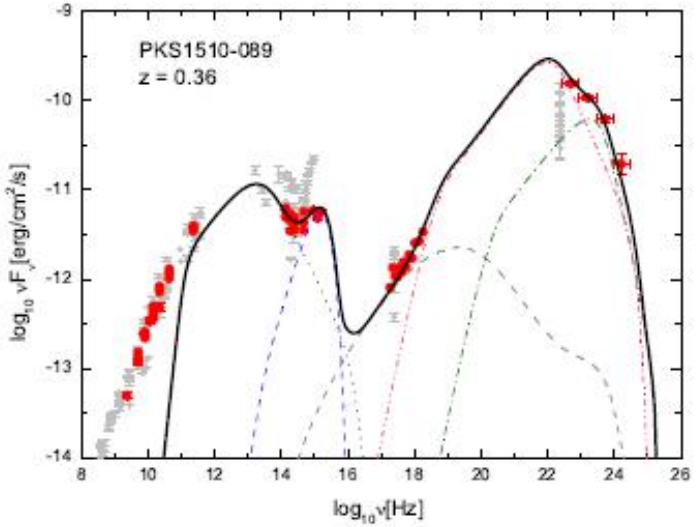

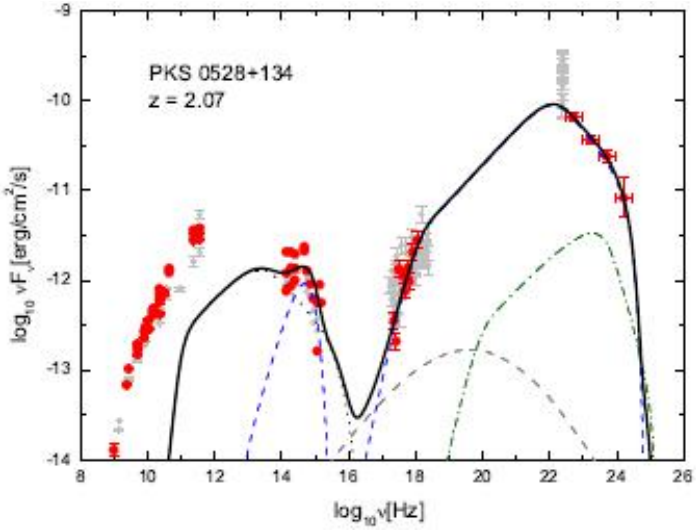

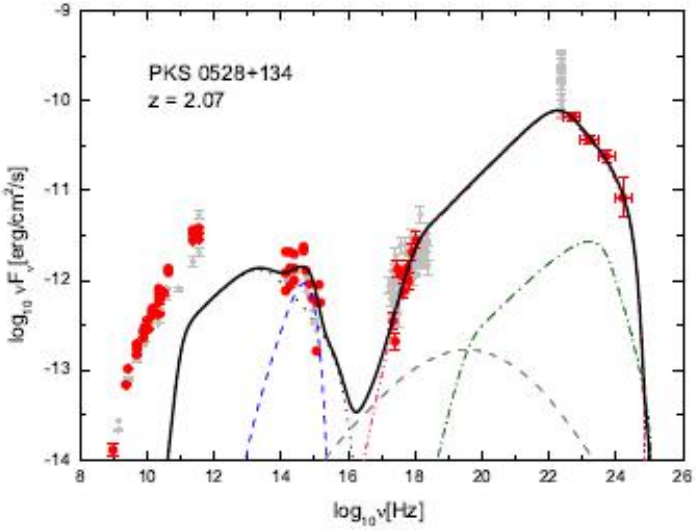

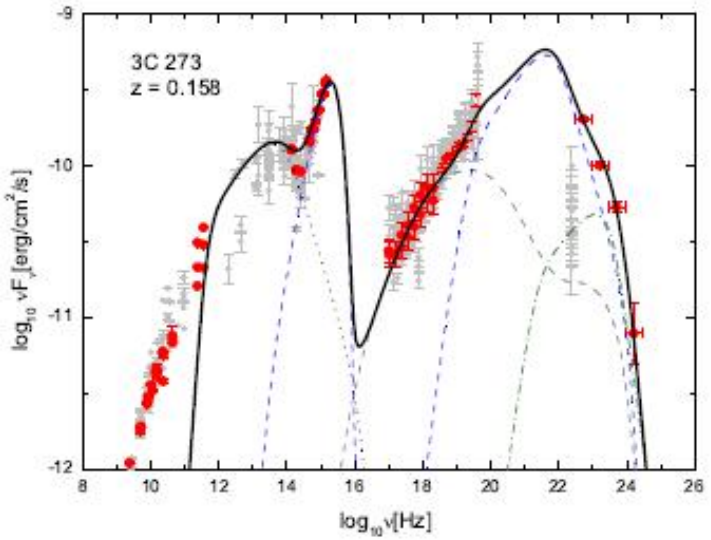
3C 273
z = 0.158
log10 vFv [erg/cm2/s]
log10 v[Hz]

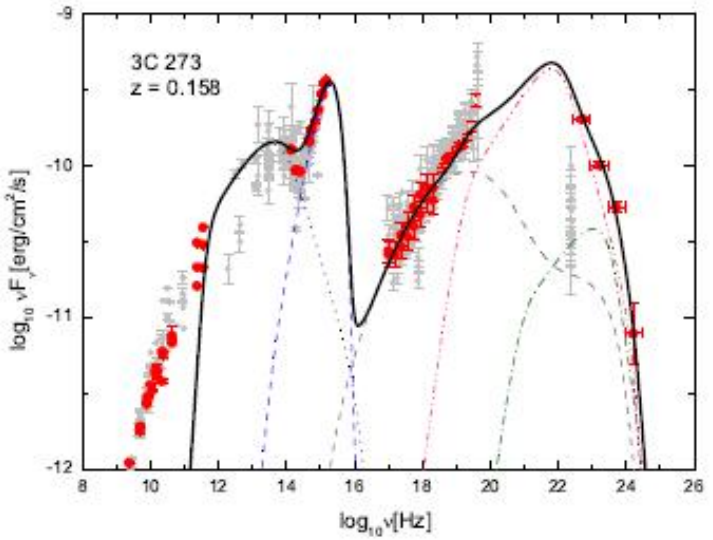
3C 273
z = 0.158
log10 vFv [erg/cm2/s]
log10 v[Hz]

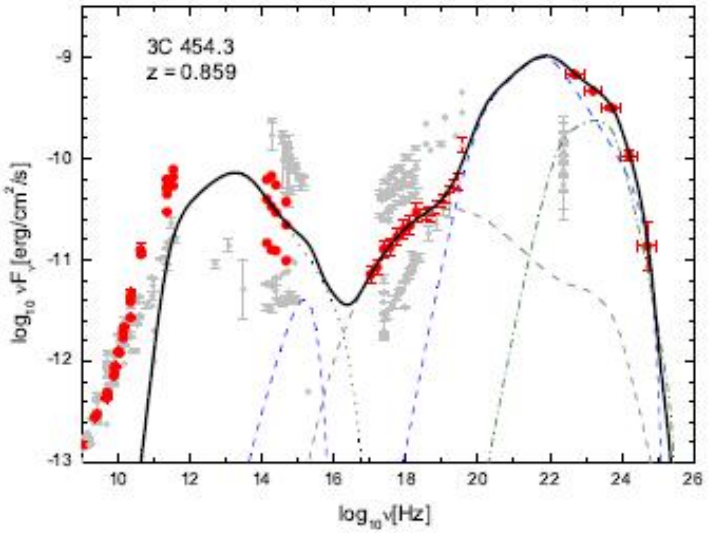
3C 454.3
z = 0.859
log10 vFv [erg/cm2/s]
log10 v[Hz]

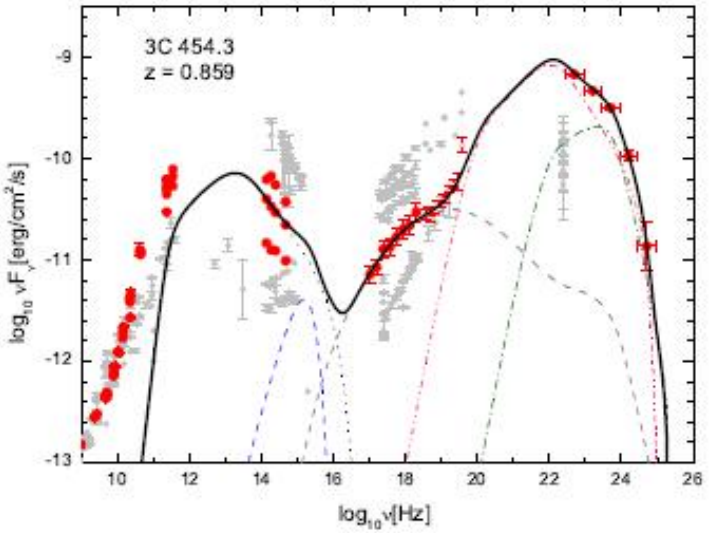
3C 454.3
z = 0.859
log10 vFv [erg/cm2/s]
log10 v[Hz]

[1] Name	[2] B' G	[3] δ_b	[4] γ'_{br} 10^2	[5] R'_b 10^{15}	[6] t_{var} days	[7] U_d	[8] T_{BLR} 10^4 K	[9] R_{BLR} 10^{-1} pc	[10] T_{DT} 10^2K	[11] R_{DT} pc	[12] P_B 10^{45}	[13] P_r 10^{45}	[14] P_{par} 10^{45}	[15] P_j 10^{45}
S4 0133+47	0.66	31.63	10.94	27.06	0.61	0.028	2.62	0.87	1.91	2.22	1.19	0.3/0.29	15.02	16.51/16.50
PKS 0208-512														.15/50.88
PKS 0227-369														.29/149.80
4C 28.07														.21/193.80
														.83/25.22
														.65/317.01
														.51/35.40
														.13/150.1
														.80/24.69
														.16/141.47
														.08/15.07
														.19/67.02
														.28/218.11
														.69/75.37
														.19/9.73
														.20/27.08
														.63/22.38
														.34/31.76
														.30/41.64
														.15/12.26
														.83/19.24
														.11/5.05
														.45/65.43
														.77/3.10
														.11/58.58
														68/106.31
														.44/6.26

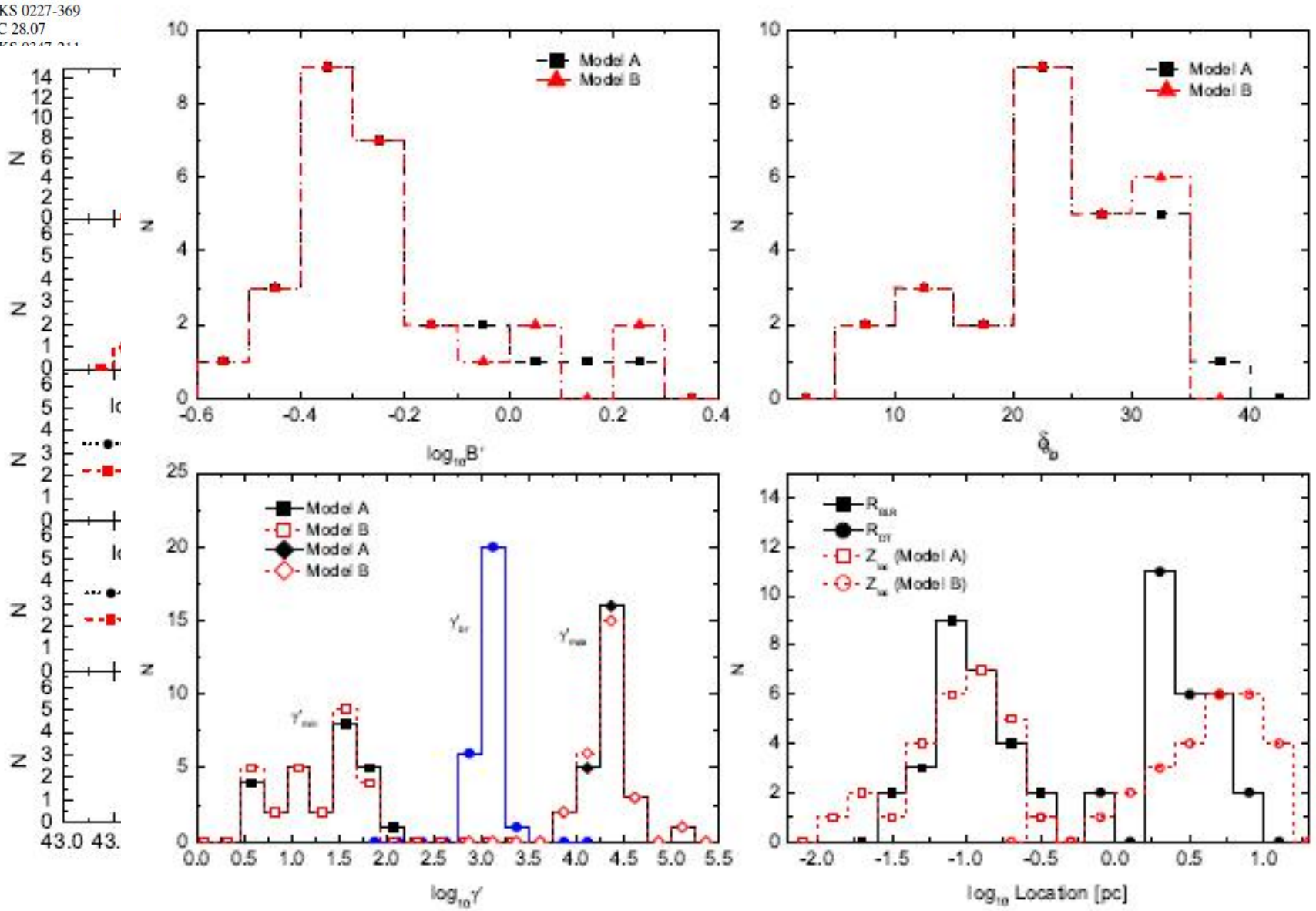

$$PDF(x) = \frac{1}{2\pi} e^{-\frac{(x-\langle x \rangle)^2}{2\sigma^2}},$$

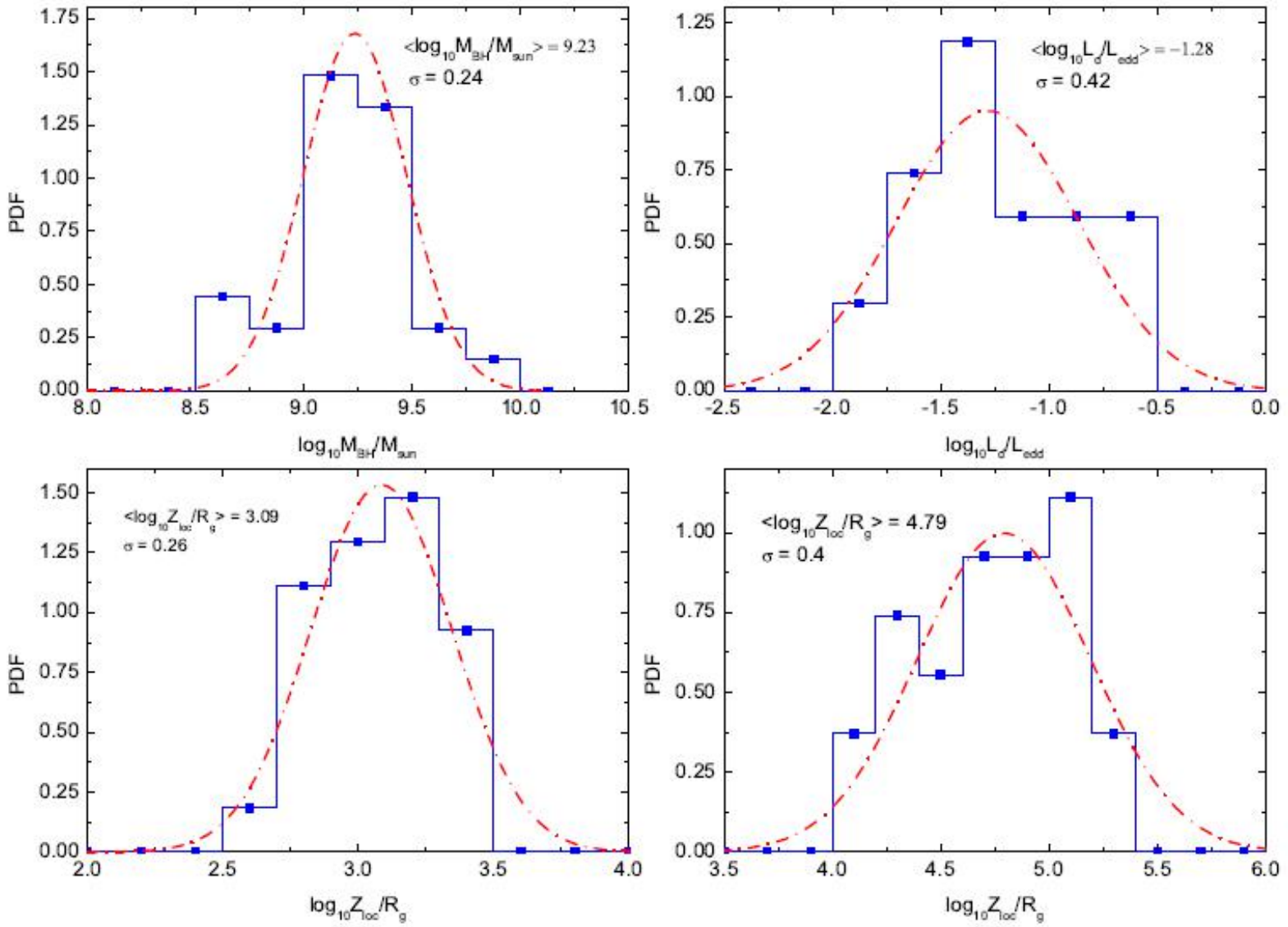

- 如果不考虑外部环境的几何结构，仅通过能谱拟合可能难以有效的限制辐射区的位置。
- 如果伽玛射线产生于 $500-4\times10^{4}R_g$ 之间，宽线区和尘埃可能都具有平的几何结构，并且它们之间可能没有缝隙。我们认为辐射区很可能在 $2\times10^{3}-4\times10^{4}R_g$ 且峰值位于 $10^{4}R_g$ 。

Summary and Outlook

- 耀变体是目前各波段观测的重要目标；
- 耀变体在全波段所具有的剧烈光变及其特性，使其成为研究喷流物理机制最重要的对象；
- 耀变体的光变机制，能谱特性及高能辐射机制仍然是目前AGN的研究热点；高能辐射及相关的物理过程可以了解其光变本质、能量耗散及粒子加速机制、辐射区环境等基本问题。
- 耀变体是极可能的河外宇宙线源
- ……

Outlook

1. Period variability

Long-term radio/optical light curves of blazars possible periods several years (OJ 287, PG 1302-102, 3C 345, AO 0235+16, 3C 273, BL Lac...)

Short-term optical/X-ray/TeV light curves of blazars possible periods of several tens of days (Mkn 501, Mkn 421, PKS 2155-304, 3C 66A, S5 0716+714 , OJ 287, …)

name	redshift z	periods P_{obs}	$(m+M)/10^8\,M_\odot$	P_k [yr]	$d/10^{16}$ cm	$\tau_g/10^8$ yr
Mkn 501	0.034	23.6 d (X-ray) ~ 23 d (TeV) 10.06 yr (optical)	(2-7)	(6-14)	(2.5-6)	≤ 5.5
BL Lac	0.069	13.97 yr (optical) ~ 4 yr (radio)	(2-4)	(13-26.1)	(4.8-9.7)	≤ 29
3C 273	0.158	13.65 yr (optical) 8.55 yr (radio)	(6-10)	(11.8-23.5)	(6.5-12)	≤ 3.5
OJ 287	0.306	11.86 yr (optical) ~ 12 yr (infrared) ~ 1.66 yr (radio) ~ 40 d (optical)	6.2	(9.1-18.2)	(5.5-8.8)	≤ 1.7
3C66A	0.444	4.52 yr (optical) 65 d (optical)	≥ 1	(3.1-6.3)	≥ 1.5	2.08
0235+16	0.940	2.95 yr (optical)? 8.2 yr (optical)? 5.7 yr (radio)	≥ 1	(1.5-3.1)	≥ 0.95	≤ 0.3

1. specific disk instabilities
2. internal jet rotation, jet precession, helical structure, resulting Doppler magnification factor changes periodically, no need for intrinsic variations in outflows and efficiency);
3. orbiting disk hot spots;
4. low frequency gravitational wave emission and may have associated PeV neutrino emission (Padovani & Resconi 2014).

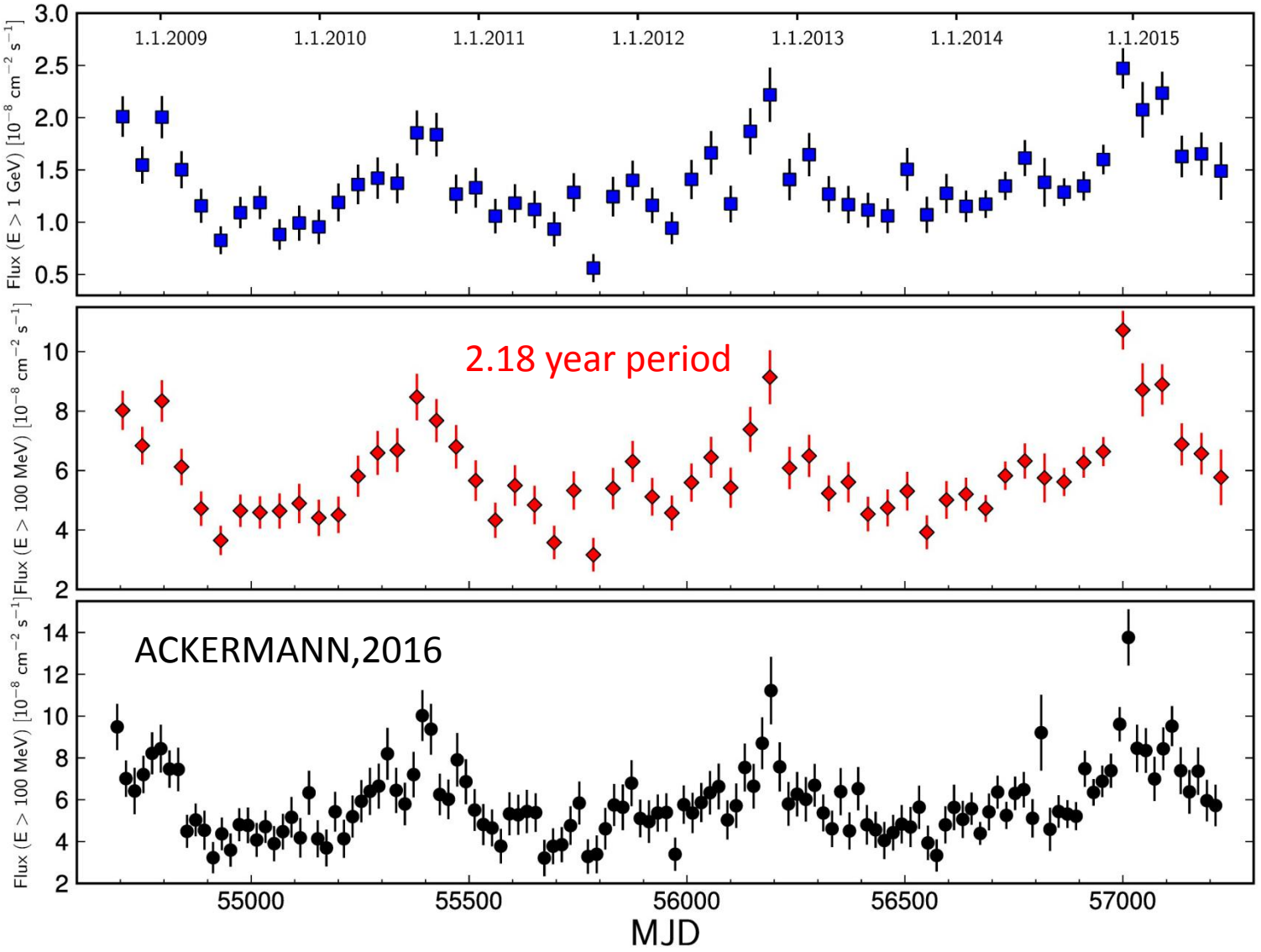

Fermi LAT -ray lightcurves of PG 1553+113 over 6.9 years, from 2008 August 4 to 2015 July 19. The lightcurve above 1 GeV is shown with a constant 45-day binning (top panel); two light curves above 100 MeV are shown, with 45- and 20-day binning (middle and bottom panels)

2. The emission model. The source of seed photons for IC scatering to γ-ray energies remains unresolved.

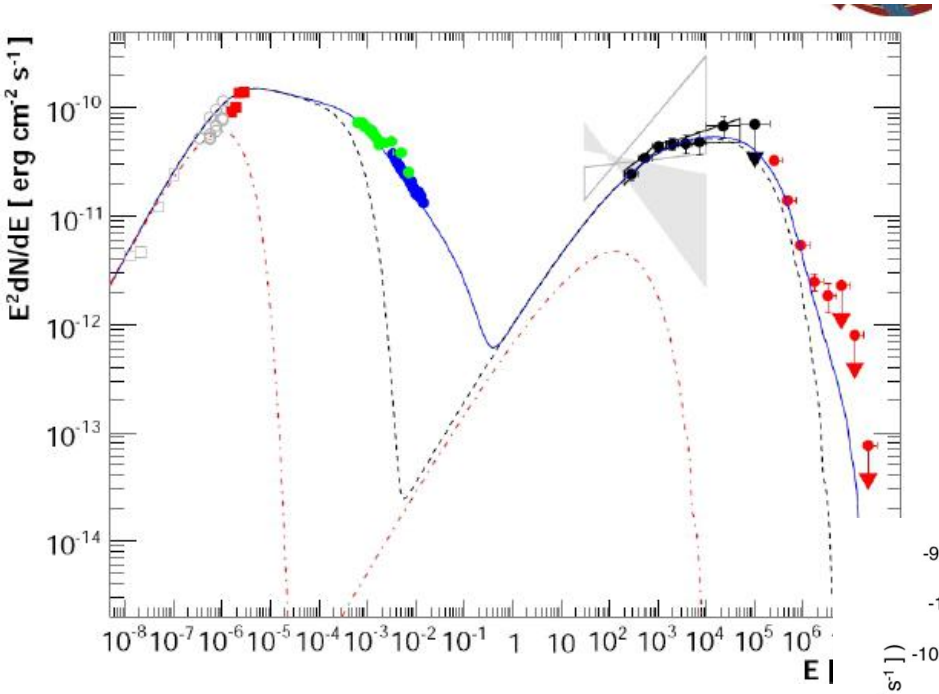

Multifrequency analysis is now powerful thanks to the Fermi 7+ years era.

LHAASO will extend multifrequency analysis to higher energy of a fewer hundred TeV.

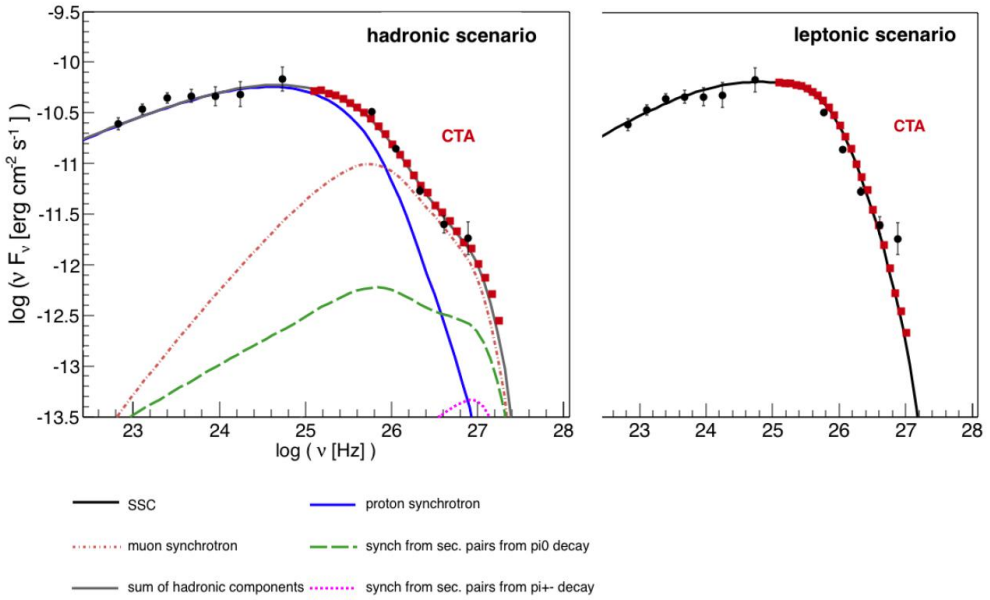

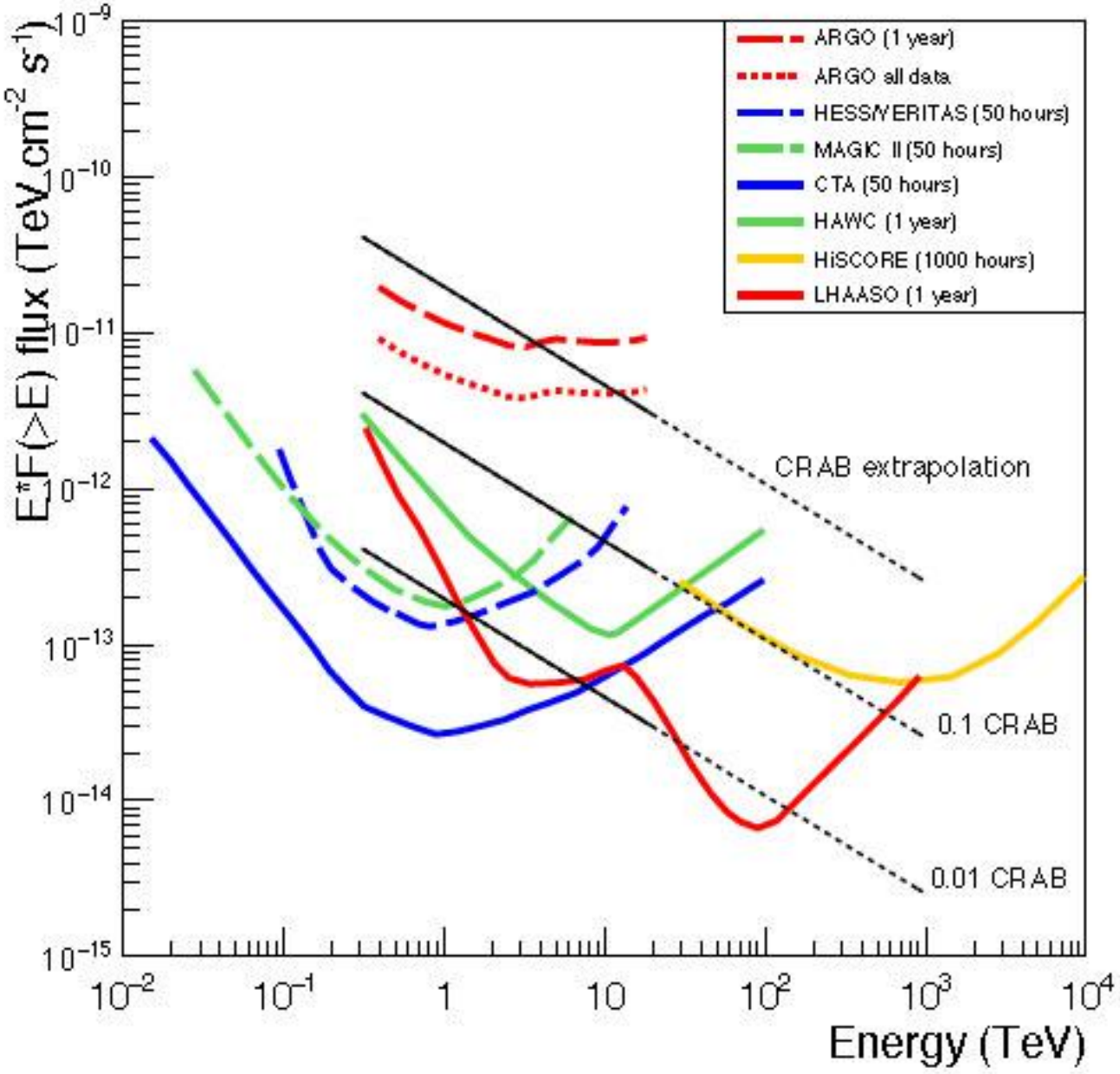
ARGO (1 year)
ARGO all data
HESS/VERITAS (50 hours)
MAGIC II (50 hours)
CTA (50 hours)
HAWC (1 year)
HiSCORE (1000 hours)
LHAASO (1 year)
CRAB extrapolation
0.1 CRAB
0.01 CRAB
E*F(>E) flux (TeV cm^-2 s^-1)
Energy (TeV)

Thank You!